Effects of salinity on the onset of elastic turbulence in swirling flow and curvilinear microchannels

Guice Yao [1,2], Jin Zhao [1], Haie Yang[2], Maje Haruna[1], Dongsheng Wen [2,1]*

[1]The University of Leeds, Leeds, LS2 9JT, United Kingdom
[2]Beihang University, 100191, Beijing, P. R. China

ABSTRACT

Elastic turbulence, which is sensitive with geometry and polymer itself, is capable of leading to improved performance of mixing, hear transfer and even oil recovery. Recently, the rheological properties of polymer solutions showed significant effects on the onset of elastic turbulence or instability. However, the variations of rheological properties based on polymer sensitivities such as salinity and its corresponding effects on the elastic turbulence have not been investigated. This work investigates systematically the effects of salinity on the onset of elastic turbulence in both swirling flow and curvilinear microchannels. The variations of statistical properties, such as probability distribution functions and spectra profiles of inject power, were analyzed for characterization. The onset conditions of elastic turbulence are postponed by high salinity, which was consistent with the mixing performance in curvilinear microchannel. A salinity independent power-law exponent at values of -4.3 was observed in fully developed elastic regime for all of polymer solutions. Particularly, the diffusion of fluorescein at low flow rate in microchannel is possible due to the existence of steady secondary flow before the onset of elastic instability.

KEY WORDS: elastic turbulence, salinity, viscoelastic fluids, swirling flow, microchannel, mixing.

1. INTRODUCTION

It is well known that a Newtonian fluid evolves from laminar to turbulence when the Reynold number exceeds a critical value so that the inertial effects could overcome the dissipation to induce the flow perturbations [1]. Unlike the Newtonian fluid, the viscoelastic fluid, which is normally composed by adding small amount of polymers in, exhibits dramatical non-Newtonian phenomena due to the elastic nonlinearity caused by polymer relaxation [2]. This elastic nonlinearity is characterized by a normalized Weissenberg number, defined as $Wi=\gamma\cdot\lambda$, where γ is the shear rate applied to the flow and λ is the polymer relaxation time. In particular, when the inertial effects are unimportant at vanishing Reynold number, the viscoelastic fluids are pronounced to induce purely elastic instability at $Wi > 1$ [3-5], and with further increase of the value of Wi, the flow is excited to a so called elastic turbulence regime [6, 7].

The first experiment on elastic turbulence was conducted by Groisman and Steinberg under von Karman swirling flow between two disks [8]. Three main features, both of which are analogous to hydrodynamic turbulence, were found for this turbulent-like flow: pronounced growth of flow resistance, algebraic decay of angular velocity spectra over a wide range of time scales and orders of magnitude more efficient mixing performance compared with Newtonian solvent solely. Later, the elastic turbulence was also observed in Couette-Taylor geometry and curvilinear channel [9, 10]. Sequences of transition profiles from the onset of elastic instability to elastic turbulence regime were systematically investigated as followed [11]. A key quantitative property for the elastic turbulence is the exponent value of the power-law spectra which is significantly different from that of the inertial turbulence of -5/3 [12]. A value in the regime of -3 ~ -4.3 can be regarded as a signal of the occurrence of the elastic turbulence [10, 13-15].

Because of the low Reynold number flow instability, elastic turbulence could have many potential applications. It was found that the elastic turbulence could lead to efficient mixing performance as aforementioned above [9, 16, 17]. For immiscible fluids, such as oil emulsification [18], elatic turbulence contributed to enhanced oil recovery during the viscoelastic polymer flooding stage[19-21]. This elastic perturbation was also proved to be capable of significantly enhancing heat transfer performance both in swirling flow and curvilinear flow [22-27]. In spite of its great potential, the basic knowledge of elastic turbulence is still not sufficient to provide a detailed mechanism, especially for the onset conditions.

Many works related to elastic turbulence have been investigated over the last two decades. The onset of elastic turbulence shows great dependence on the experimental geometry [10]. Even with same apparatus, such as swirling flow, the aspect ratio affects the onset of elastic turbulence pronouncedly [28]. A skewness of the probability density functions (PDFs) of injected power profile was observed in elastic regime, which was mainly attributed to the mixing layer, where excessive elastic stresses were supposed to be injected into bulk [14, 29-31]. This skewness, however, showed independent relationship with polymer concentration when the concentration was lower than 900 ppm [15]. When the scale down to micro level, especially in curvilinear channel, the elastic turbulence becomes more challenging to characterize. The onset of elastic turbulence in such geometries was normally characterized based on the mixing performance coupled with axial velocity profile conducted by a micro-PIV (μ-PIV) system. With more advanced Digital Holographic microscope, a three-dimensional velocity field was plotted [32, 33]. It was found that the elastic stresses were not saturated in elastic turbulence regime in serpentine channel, which was mainly due to the boundary layer in bounded flow channels [34]. In addition, unlike the swirling flow, a steady secondary flow was observed in such a geometry before the onset of elastic turbulence [35]. Besides these standard geometries related to rheometer, elastic turbulence was also triggered in any other geometries, such as porous media [19-21, 36, 37], cross-slot channel [38] and viscous disk pump [39, 40]. From these curvilinear geometries, the curvature of the geometry was regarded as an essential condition to induce elastic turbulence or instability. The effects of curvature were systematically analyzed by Zilz et.al [41].However, this assumption was controversial since the elastic turbulence was also triggered in a straight channel by inserting numbers of obstacles in the center [42-44]. A direct numerical simulation of three-dimensional flow in parallel plates also showed different results [45]. Until now, the roles of curvature played during the elastic instability transition are still unclear and more developed future works are emergently required.

Indeed, besides the geometry, the physical properties of polymer solution itself showed significant effects on the onset of elastic turbulence. The polymer type, concentration, solvent type and so on are both related to the occurrence of elastic turbulence. Different polymers such as PAM, PEO[18, 46], DNA [47]and hydrolyzed PAM (HPAM) [19-21, 36, 48], due to the discrepancy of polymer relaxation time, chain length and molecular weight, have different onset values of elastic turbulence. Not only for polymers, it was found that micelles could induce similar elastic turbulence phenomena under some conditions [49-52]. Particularly, studies demonstrated that the rheological properties of polymer solutions, such as shear thinning [18, 48, 53], also influenced the onset condition even with same type of polymer. However, these various rheological properties were ascribed to the variations of solvent or polymer concentration.

In many potential applications, such as HPAM for enhanced oil recovery, the complicated water chemistry (such as pH, ionic strength and dissolved organic matter contents and properties) would affect the performance significantly. For HPAM, because of the charged carboxylate functional groups along the backbone, its rheology is sensitive to many factors, among which salinity is one of the most noteworthy [54]. The effects of such sensitivity on the onset of elastic turbulence have not been investigated and revealed, which forms the motivation of this work. In addition, the transition

from laminar to elastic turbulence was accompanied by a coil-stretch transition observed by Gerashchenko [55]. HPAM could have different morphologies under different salt concentrations, as revealed recently by experiments and simulations [56-58]. However, how such variations of initial configurations would affect the elastic turbulence is still unclear. Aiming to address these issues, this work perfoms a systematic study to reveal the influence of salinity on the onset of elastic turbulence in two configurations: swirling flow and curvilinear microchannel flow. This work was conducted as followed. The rheology variations with different salinity were first investigated, followed by experiments studying the consequent effects on elastic turbulence in swirling flow. The statistical properties of injected power were systematically analyzed. Similar working fluids were applied in a curvilinear microchannel to study the mixing performance with different salinities and the discrepancies between these two geometries were discussed.

2. EXPERIMENTAL MEASUREMENTS

2.1 Experimental setup

The schematic diagram and experimental system are shown in Fig. 1. The polymer solution was held in a stationary transparent cup with a flat bottom. A co-axial rotating upper plate was just touching the surface of the fluid. The transparent bottom of the cup as the lower plate was attached to the rheometer concentrically with the shaft but above the rheometer base. The upper plate was attached to the shaft of the rheometer, which allowed precise control of its rotation velocity, Ω, and measurements of the torque, T.
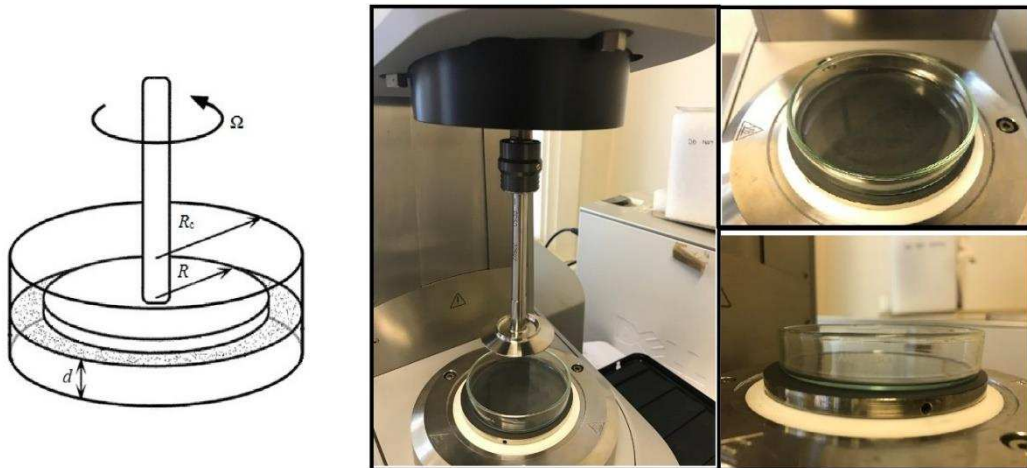

Fig. 1a The experimental swirling flow set-up

Based on previous study, the onset of elastic turbulence was sensitive to geometrical aspect ratios. When the radius of the cup, R_c, kept constant, the onset values of the relevant physical quantities such as shear rate or Weissenberg numbers increased as the gap between two plates, d, decreased. Similarly, if the distance between two plates was set as a specific value, these threshold values became higher with increasing the radius of the cup. Therefore, a small radius of the cup associated with a large gap is able to induce elastic turbulence more easily. In this study, the radii of the upper plate and the cup were chosen as R=25 mm and R_c=35 mm, respectively, and the gap between the plates was d=10 mm. The examination of the salinity effects on the mixing performance are conducted in a curvilinear channel. Such a geometry is selected not only because of its This popularity in microfluidic systems, but also allowing extended continuous experiments with well controlled initial conditions. The experimental system and the structure of the channel is drawn in the snapshots is shown in Fig.1b. shown latter. It consists of a sequence of smoothly connected half-rings with square cross-section. The total length of the channel is 121mm and the width (depth) is 640 μm. The mixing experiments were conducted by injecting two liquids simultaneously by a syringe pump at a specific flow rate.

Chemical composition of these two liquids are same but one of those was dyed by fluorescein rhodamine B. The mixing performance was observed by a CCD camera from the top of the channel.

2.2 Working fluids

Two types of working fluid were used in this study, Newtonian fluid and viscous elastic fluid. The Newtonian fluids, regarded as base fluids, were 65% sucrose aqueous solutions with two different concentrations of sodium chloride (NaCl), 0% and 1 %, respectively (referred to "sucrose solution" here after). The addition of NaCl was conducted to exclude the effects of salinity on the base fluid. The viscous elastic fluids were prepared based on 65% sucrose solutions with different concentrations of HPAM (MW: 22 M g/mole) and NaCl (referred to "HPAM solution" here after). Three dilute polymer concentrations from 100 to 300 ppm were conducted to reveal the effects of polymer concentration on the onset of elastic turbulence as well as determine an optimal concentration for the following study on the effects of salinity. A wide range of NaCl concentrations, from 0.01% to 1% were investigated. Hereinto, 65% sucrose was conducted as both the base fluid and the solvent of the HPAM solutions since it could maximise the relaxation time of the solution and minimise the Reynolds numbers, thereby the flow instabilities were attributed to elastic effect rather than inertial effect.
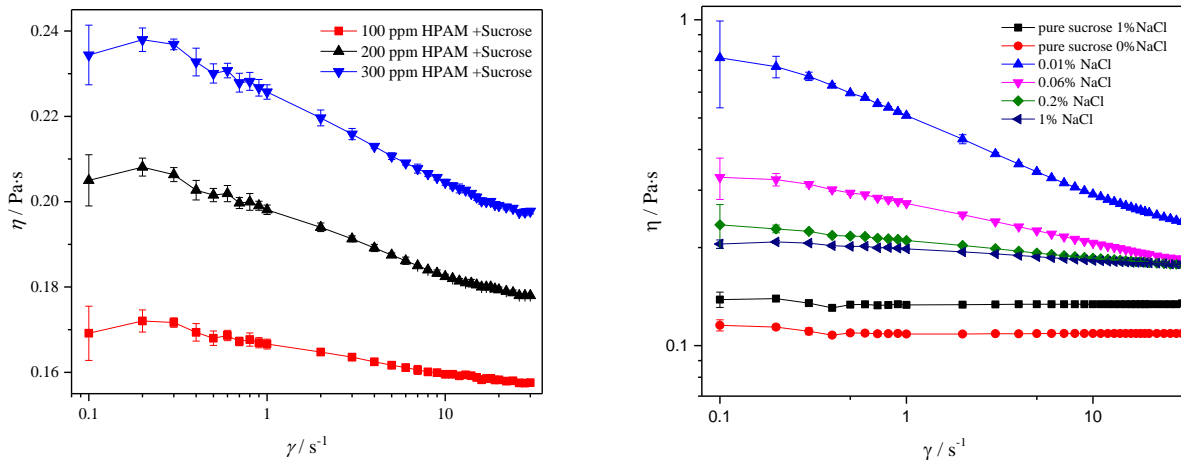

Fig. 2 Viscosity profiles of working fluids applied during experiments

The viscosities of working fluids were measured by cone and plate geometry of a MCR 301 rheometer (Anton Paar, Austria) under the strain-controlled mode at 25 ℃, as shown in Fig. 2. The sucrose solutions show shear constant phenomenon while a shear thinning property is observed for polymer solutions. With higher polymer concentration and low degree of salinity, the viscosity becomes smaller. It need to be noticed that the shear thinning phenomenon disappear gradually as the salinity increases. Indeed, both the polymer concentration and the degree of salinity have significant effects on the polymer relaxation time.
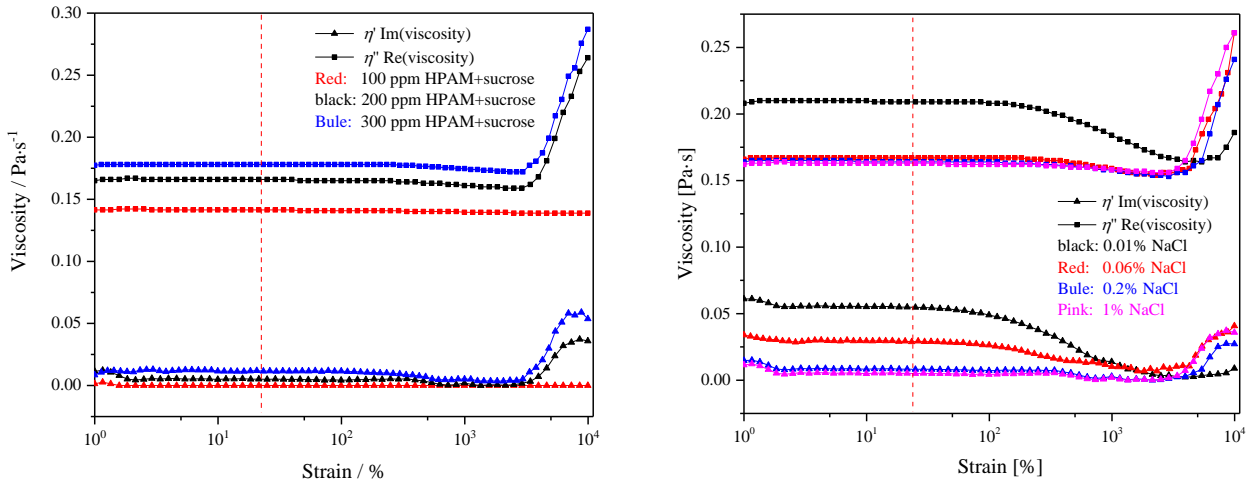
Fig.3 polymer stability as a function of strain rate for working fluids

The polymer relaxation time, λ, was measured in the oscillatory test mode. The in-phase and out-of-phase viscosity of polymer solution, η' and η'', respectively, were measured in long series at different angular frequencies ranging from 0.6 to 50 rad·s^{-1}. The amplitude of strain rate during oscillatory test was determined as 20% according to Fig. 3. Same procedures were applied to the pure sucrose solutions and the η_s' and η_s'' were measure as well. The values for the polymer in-phase and out-of-phase viscosity were calculated as $\eta_p'=\eta'-\eta_s'$ and $\eta_p''=\eta''-\eta_s''$. The polymer relaxation time then was obtained as:

$$\lambda = \lim_{\omega \to 0} \left[\frac{1}{\omega} \left(\frac{\eta_p''(\omega)}{\eta_p'(\omega)} \right) \right]$$

(1)

The relaxation time for each sample was predicted by fitting the experimental results at the angular frequency close to zero as performed in Fig 4. It is found that increasing the polymer concentration results in the increase of polymer relaxation time. In contrast, an increase of the degree of salinity causes a reduction of the polymer relaxation time.
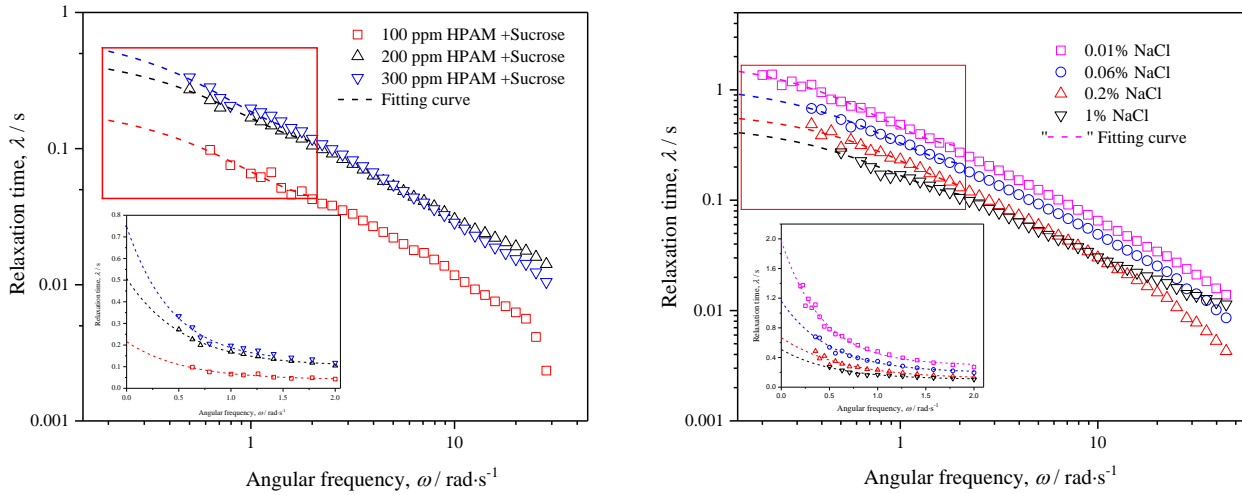

Fig. 4 polymer relaxation time profiles for different working fluids

2.3 Data analysis details

For the swirling flow between two plates, the bulk shear rate is significant inhomogeneous. When a narrow gap applied, d/R << 1, the shear rate along the axial direction can be regarded as constant and the radial shear rate varies from zero at r=0 to maximal value of ΩR/d at r=R. The average shear rate over the surface of upper plate is then calculated as 2ΩR/3d. However, for the case with large gap, the shear rate becomes strong non-homogeneous along the axial direction. In this case, the average shear rate is no longer equal to 2ΩR/3d and should be several times larger. To estimate the real shear rate of the experimental setup, 65% pure sucrose solution was tested in both narrow gap (1 mm) and

wide gap geometry (14 mm). It showed that the average shear rate γ_{av} was proportional to Ω, being $\gamma_{av}=3\Omega R/d$ in this experimental setup.

The sharp growth of flow resistance is a key feature of the elastic turbulence. The ratio of the average stress, τ_{w}, at the upper plate to the imaginary stress in the laminar flow, τ_{w}^{lam}, at the same angular velocity is a suitable parameter to characterise this growth. The average stress of the upper plate was measured by rheometer automatically while the imaginary laminar stress would depend on an average shear rate and viscosity of the polymer solution, defined as $\tau_{w}^{lam}=\eta(\gamma_{av})\ \gamma_{av}$. To characterize the Weissenberg number and Reynolds number, a simple expression $\Omega R/d$ was used as a characteristic shear rate. Therefore, the Weissenberg number (Wi) and Reynolds number (Re) can be calculated as:

$$Wi = \lambda \frac{\Omega R}{d} \qquad (2)$$

$$Re = \frac{\Omega R d \rho}{\eta} \qquad (3)$$

3. RESULTS AND DISCUSSIONS

3.1 Effect of polymer concentration on the onset of elastic turbulence

The Fig. 5 shows the dependence of normalized flow resistance on the shear rate for three polymer solutions with different concentrations. The shear rate was increased gradually in time (1000 points per decade) from 0.1 to 20 s^{-1} with each shear rate being held by 5s. A sharp growth of stress ratio has been observed in higher polymer concentration, which indicates a strong non-linearity in the swirling flow and confirms that the HPAM is indeed able to induce the elastic instability at low Reynold numbers. Under the same applied shear rate, the pure Newtonian fluid is remaining in laminar regime without any sharp variations during the experimental test, which indicates that the inertial effect in this situation can be omitted and the flow resistance growth is solely driven by the elastic instability, similar to previous studies [ref].

Growth of the flow resistance is affected significantly by polymer concentration. At low concentration such as 100 ppm in this study, the polymer elasticity is too weak to induce the flow instabilities at such applied shear rates, showing similar phenomenon as the sucrose solution. With increased polymer concentration, three flow stages are evolved as laminar state, elastic instability regime and elastic turbulence regime, respectively. The onset values of elastic instability are dependent on polymer concentrations. With a higher concentration, the polymer solution tends to be unstable easily and the stress ratio saturates at higher values. The reasons are attributed to the large amount of polymer molecules in solutions, which limits the degree of the perturbations induced by polymer conformation feedback. Therefore, to get a same perturbation, for less polymer concentration, a single polymer chain should contribute more instabilities. Similarly, when the elastic stress provided by a single polymer chain saturates, the total shear stress growth is smaller.

The quantitative results are listed in Table 1. Although the threshold shear rate increases with the reduction of the polymer concentration, the polymer relaxation time decreases as well, making the critical Weissenberg numbers of the onset of elastic instability are similar, 5.6 and 5.8 s^{-1}, respectively. This agrees well with the investigations conducted by Jun [ref] that the elastic instability occurs at higher Weissenberg number in extremely low polymer concentration and then keeps constant at some range of polymer concentrations showing the independent relationship.
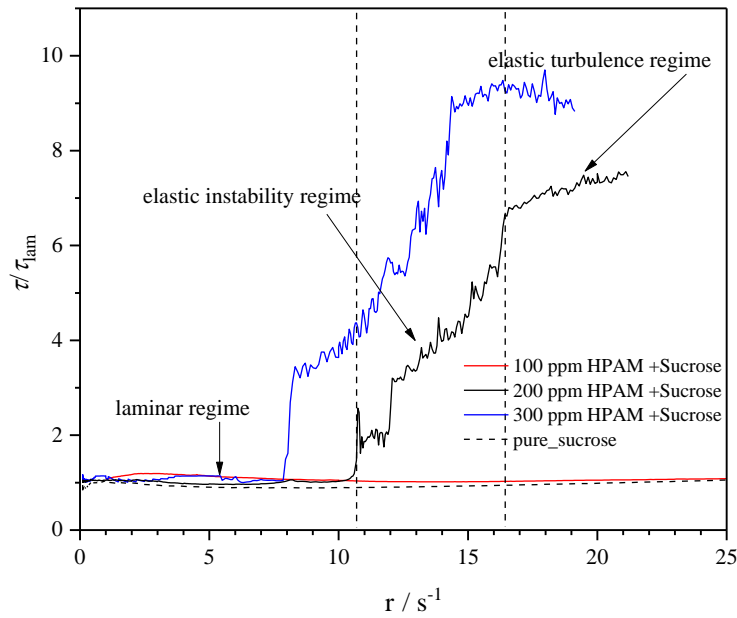
Fig.5 The ratio of the average stress at the upper plate, τ, to the stress, τ_w^{lam}, in imaginary laminar shear flow as a function of the shear rate, γ with different polymer concentration

Table 1 Properties of polymer solutions and flow characteristics: γc is the threshold shear rate of the elastic instability; λ is the relaxation time of the polymer solutions; Wic is thee threshold Weissenberg number of the elastic instability

c (ppm)	sucrose	100	200	300
γ_c (s^{-1})	--	--	10.8	7.8
λ (s)	--	0.22	0.52	0.75
Wi$_c$	--	--	5.6	5.8

3.2 Effect of salt on the onset of elastic turbulence

The onset of elastic instability is associated with the coil-stretch transition of polymer molecules, which is likely be affected by the polymer's initial conformation. Compared with pure polyacrylamide (PAM), HPAM is different since part of arylamide monomers are substituted by acrylate, along which the carboxyl function group is sensitive with cations. With various amount of salts being added into polymer solutions, the onset values of elastic instabilities should be different. In this section, the effects of salinity on the onset of elastic turbulence are discussed in detail.
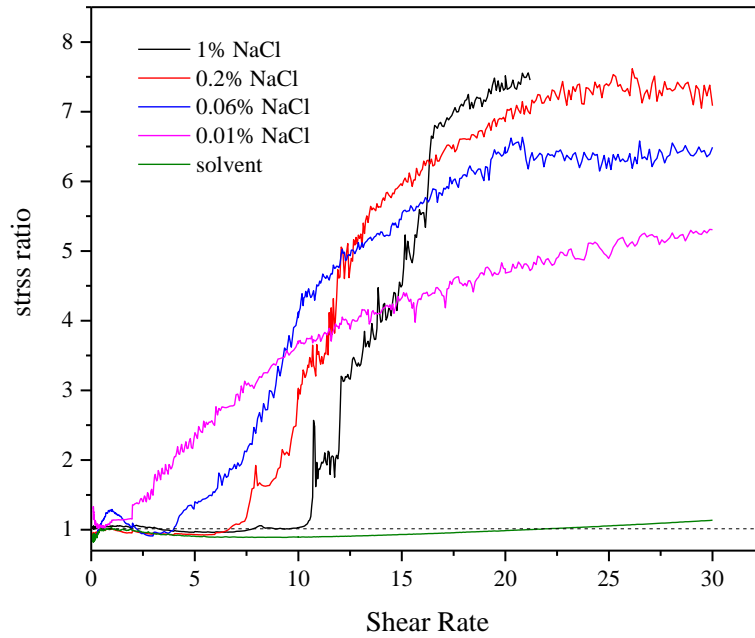
Fig. 6 The ratio of the average stress at the upper plate, τ, to the stress, τ_w^{lam}, in imaginary laminar shear flow as a function of the shear rate, γ with different salt concentration

The variations of stress ratio with different salinities are shown in the Fig. 6. Both curves of polymer solutions are followed the rules mentioned above: increase rapidly over a value of shear rate and saturate at a higher value. With the same controlled parameters, however, the Newtonian solvent stayed in the laminar state, indicating the inertial effect was negligible . It is much more difficult to induce elastic instability at higher salt concentrations, which mainly attributed to two main reasons: the reduction of polymer relaxation time and the shielding effect on the negative charged polymer backbone. As shown in Fig. 7, increasing salinity decreases the polymer relaxation time correspondingly. Based on the definition of the Weissenberg number, if a small relaxation time is provided, a high shear rate should be applied to trigger the flow instability. The shielding effect, caused by the additive cations, forces the polymer configuration staying in coil state. In order to elongate the polymer chain from coil state to stretch state, additional power is required to overcome this electronic suppression. With the increase of the salinity, more cations dense around the polymer chain, resulting in more intensive shielding force and leading to higher shear rate to induce the elastic instability. Besides, the addition of salt influences the solvent quality and then even collapse denser coil state [59, 60]. With the combined influences of these factors, the threshold values of Weissenberg number at the onset of elastic instability for different polymer solutions are demonstrated in Fig. 7. The critical Weissenberg number (Wi_c) slightly increases with increasing the degree of salinity of polymer solutions but keep in same order of magnitude from approximately 3.8 to 5.4 with salinity ranging from 0.01% to 1%, respectively.

In addition, the transition from laminar state to elastic turbulence regime becomes shorter with the increase of the salinity. This phenomenon is also attributed to the reduction of the polymer relaxation time and viscosity of polymer solution. Polymer molecules are required less time to equilibrate and are more disperse with high salinity, which makes the transition shorter. Besides, it is also indicated that polymer solution with concentrated salts has a better performance of flow intensification in the regime of elastic turbulence. Indeed, similar averaged shear stresses over the upper plates were obtained for all polymer solutions. However, the addition of salts diminished the viscosity of polymer solutions, which resulted in lower imaginary laminar shear stress and thereby performing higher stress ratio. In other words, the shear stress in elastic turbulence regime is constituted of initial viscous force and flow friction based on flow instabilities. With the same total shear stress, the polymer solution with lower viscosity holds better performance of flow intensification.
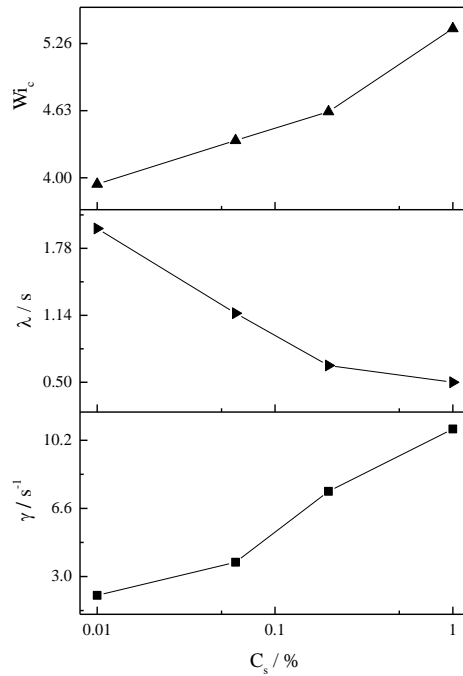
Fig 7 Salinity effects on the threshold properties of polymer solutions at the onset of elastic instability

The fluctuation of the injected power, defined at any case as P=T·Ω, is another main feature to characterize elastic turbulence. The time series of the injected power at different Wi under Ω controlled mode for HPAM solution with 1% NaCl is presented in **Fig. 8**. The average values of the injected power do not change significantly during the total data acquisition times, indicating that no major polymer degradation occurred. For low control parameters in laminar regime, $\gamma < \gamma_c$, the power fluctuations are only attributed to instrument noise. However, in elastic turbulence regime, the fluctuation becomes intensively and irregularly. These fluctuations of injected power reflect fluctuations of the elastic stress averaged over the upper plate, which estimate that motion of the polymer is spatially random.

For each run with specific values of C_s and Wi, the probability distribution functions (PDFs) are based on 2×10^4 measured data points evenly sampled in time (Δt=50 ms). Here, the PDFs of HPAM solution with 1% salinity as a function of shear rate is in the Fig. 9. In the elastic turbulence regime, the PDFs of the inject power fluctuations strongly deviate from the Gaussian distribution and show a left skewness, which is mainly attributed to intermittently injection of excessive elastic stresses from boundary to bulk flow [14]. This skewness becomes more dramatically as the shear rate or Weissenberg number increases. The PDFs of inject power fluctuations collapse on a single curve when normalized by their maximum value as plotted in Figure xx, where P^{rms} is the rms values.
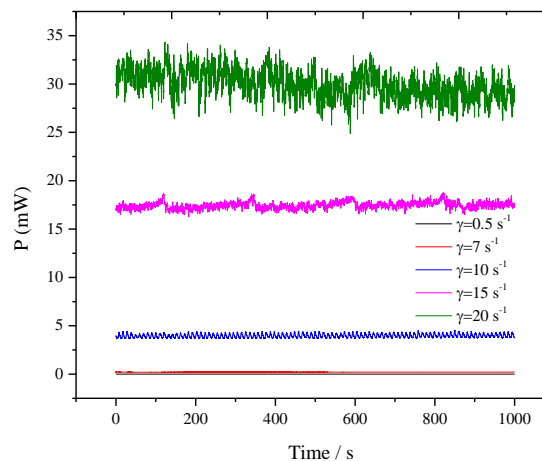
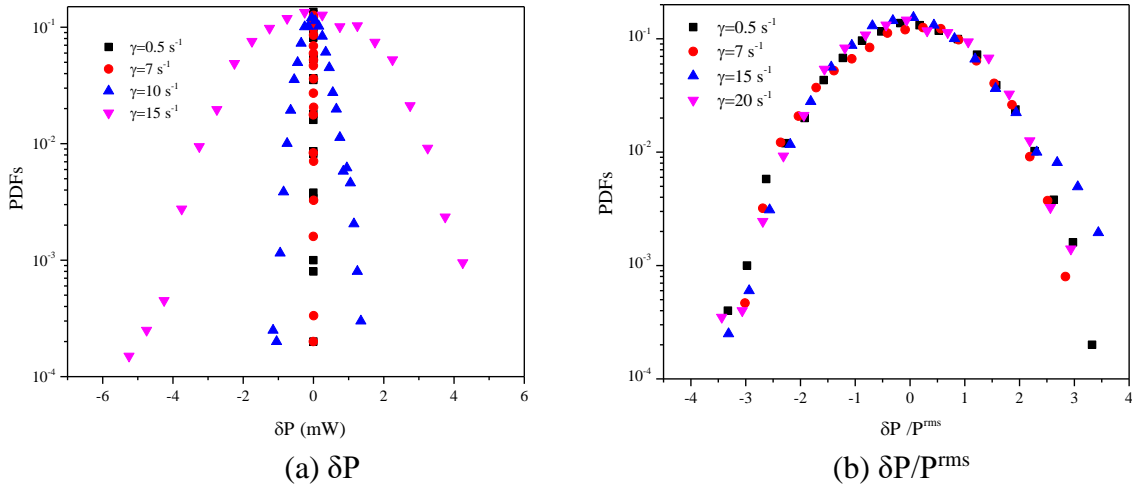Fig. 8 The time averaged fluctuations of inject power for different shear rate

(a) δP

(b) δP/P^rms

Fig. 9 PDFs of δP and δP/P^{rms} for different shear rate of HPAM solution with 1% NaCl

The normalized PDFs for salinity from 0.01% to 1% at the highest shear rate (20 s^{-1}) are presented in the Fig. 10(a). Both curves are skewed toward the negative values. It can be noticed that this skewed trend becomes slightly more dramatically with higher salinity, which also quantitatively characterized in the Fig. 10(b). Both the skewness, S, and flatness, F, for the fluctuation of inject power increase as the salinity increases. These PDFs properties indicate in turn that the polymer solution with higher salinity driving more intensive flow perturbations.
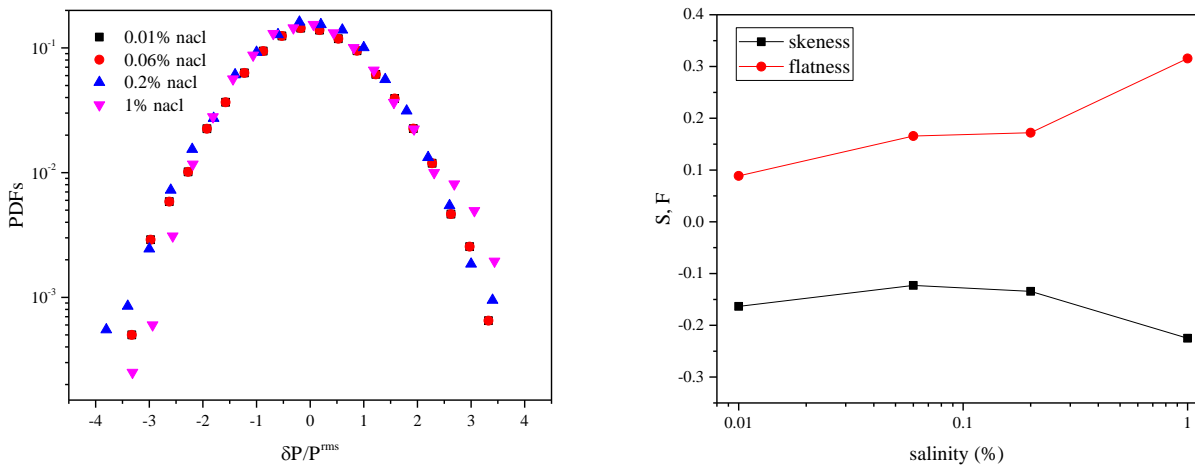
(a) PDFs of δP/P^{rms}

(b) Skeness and Flatness of PDFs as a function of salinity

Fig. 10 The statistic properties for fluctuations of inject power of HPAM solutions with different salinity

The frequency power spectra of injected power of the upper plate at different averaged shear rates are measured to reveal more detailed features of the flow dynamics. The spectra transition profile for HPAM solution with 1% NaCl is shown in Fig. 11. The curve evolves to a power-law decay pattern, $P \propto f^{\alpha}$ as the shear rate gradually increases into elastic turbulence regime and this law becomes more established at higher shear rate. The steep decays are resulted from the transfer of energy from the low-frequency modes down to high frequencies by stretching and folding of elastic stress field by a random flow. All spectrum in the elastic turbulence regime behaves similar appearance: a broad region at $f < f_{vor}$, and a steep power-law decay over decades at $f > f_{vor}$, where f_{vor} is main vortex frequency with a peak visible on the plot at $f=f_{vor}$. The f_{vor} tends to higher frequency domain region with the increase of shear rate as shown in Fig. S1, which agrees well with the previous study. Before the flow dully developed into elastic turbulence regime, the power exponent slight increases and keeps constant at the value around -4.3, which is same with the exponent obtained from Groisman and Jun of -4.3 and -4, respectively, and much larger than the one in inertial turbulence [10, 15]. The

spectrum of HPAM solutions with other degree of salinity are listed in Fig. S2-S4 in the supporting document.
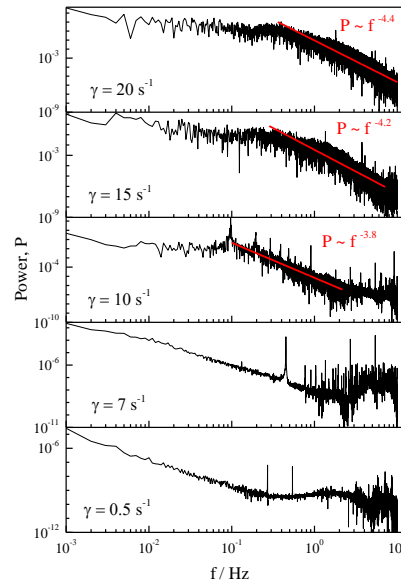

Fig. 11 The frequency power spectra of injected power of the upper plate with different shear rate for HPAM solution with 1% NaCl

The spectrum of inject power with different salinity at three shear rates are presented in Fig. 12. (the spectrum at $\gamma.=10$ s^{-1} are listed in supporting document). Through the spectrum profiles, one can see that with lower salinity, the power-law-decay phenomenon is more easily observed, which shows great consistency with the trends of stress ratio discussed above. At lower shear rate, as shown in figure xx, the power exponent increases with the reduction of the salinity and the f_{vor} moves to large frequency domain since the HPAM solutions with high salinity are not fully develop in elastic turbulence regime. However, at high shear rate, as displayed in Fig. 12(b) and Fig. S6, the power exponent is independent on salinity and keeps constant value around -4.3. The normalized peak frequency, f_{vor}/f_{rot}, as a function of Wi/Wi$_c$ is plotted in Fig. 13. As the flow evolves into elastic turbulence regime, this normalized peak frequency equilibrate toward a constant value at 0.22, which is totally same with results analyzed by Jun [61]. It shall be noticed that even at the highest shear rate, the spectrum of sucrose solution does not show any turbulent-like phenomenon, which again proves the existence of elastic turbulence and provides convincement for the results of salinity effects.
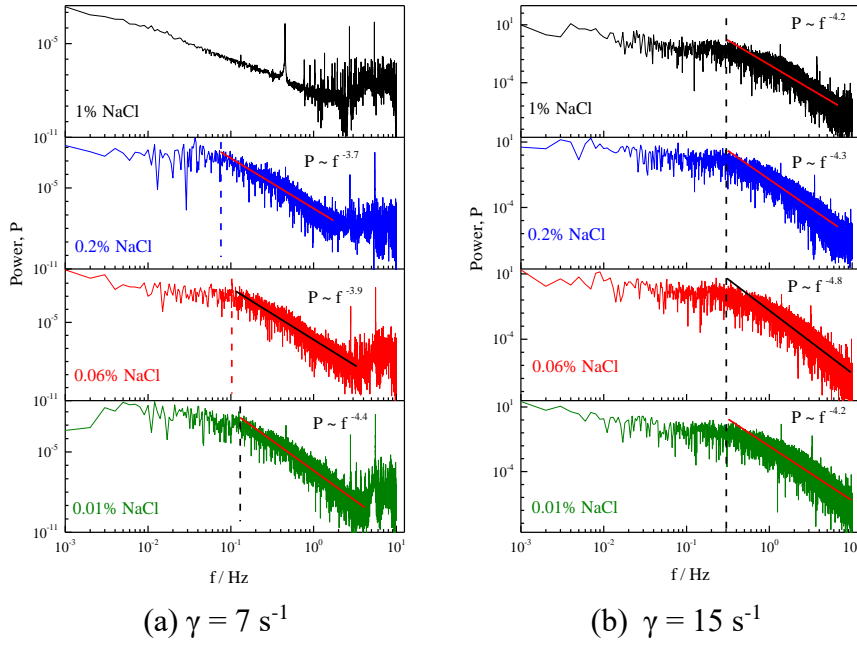
(a) $\gamma = 7\ s^{-1}$ (b) $\gamma = 15\ s^{-1}$

Fig.12 Power spectra of fluctuations of injected power of the upper plate at different salinity
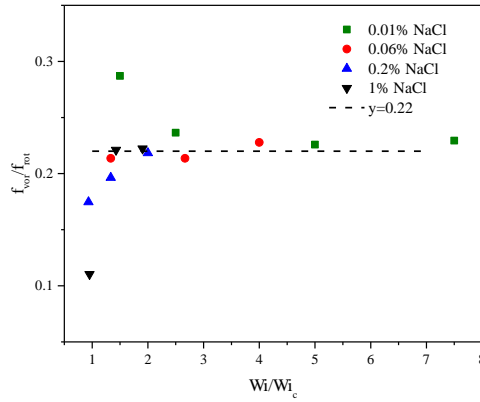

Fig.13 The normalized frequency of the main vortex f_{vor}/f_{rot} as functions of Wi/Wi$_c$ at different salinity

3.3 Salinity effect on mixing performance in microchannel

The snapshots for mixing performance of HPAM solution with 1% NaCl are partially displayed in Fig. 14. A clear interface is found between two injected liquids at the position close to the inlet at low flow rate. This interface turns to be less dramatic downstream due to the diffusion of the fluorescein caused by the slight flow instability, which induced by the curvature of the microchannel. Such an instability is too weak to trigger elastic turbulence as there is still no chaotic streamline observed. It is consistent well with the recent point view that there exists a steady secondary flow before the onset of elastic instability [35, 38]. The hysteretic transition from laminar to elastic turbulence is possible due to this steady instability. The dimensionless mixing length, defined here as the ratio of the numbers of rings with clear interface to the total rings of the microchannel, increases as increasing flow rate. This is mainly due to that the high flow rate pushes the flow passing through the channel rapidly, which results in the reduction of the dispersion of dye to the direction of cross section. The flow becomes chaotic when the flow rate reached a specific level, making the clear interface disappear suddenly even close to the inlet of the channel. This phenomenon is accompanied by a significant

streamline cross, indicating the occurrence of the elastic turbulence. Indeed, based on the previous studies [10, 42, 43] , the amounts of curvilinear rings or inserted obstacles do affect the flow dynamics. The more numbers of those the fluid flowing through, the more intensive of the flow perturbations due to the acceleration of the elastic instability. It is challenging to characterize such onset of elastic instability around outlet of the channel even with detailed velocity profile. Therefore, a simple condition at which the whole channel is fully mixed is regarded as the signal of the onset of elastic turbulence.
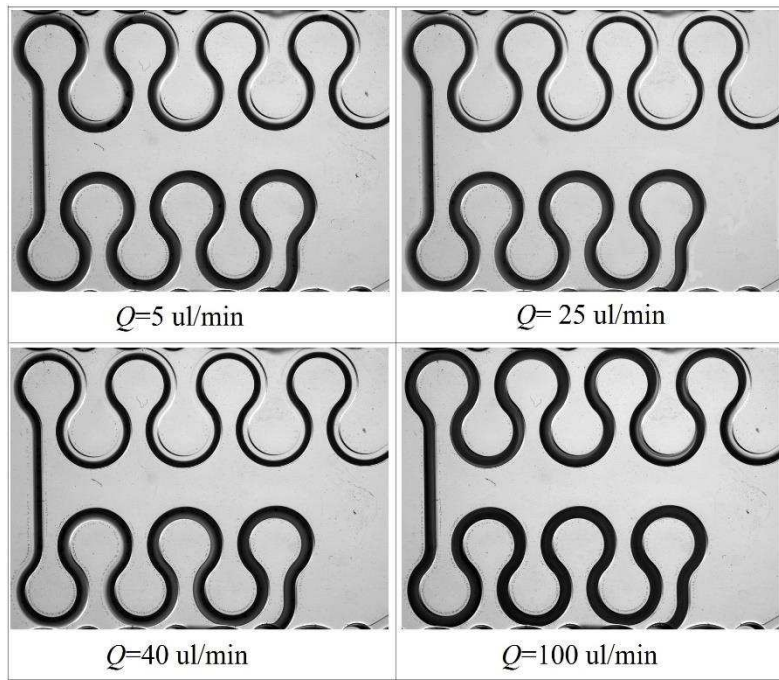

Fig. 14 snapshots of mixing performance with different flow rate of HPAM solution with 1% NaCl

Same series of salt concentration were conducted to investigate the mixing performance in the curvilinear microchannel. The variations of mixing length for HPAM solutions with different salinities are quantitatively plotted in Fig. 15, and some representative snapshots at flow rate of 20 µl/min are shown in Fig. 16 as well. The mixing length increases first then decrease sharply with increasing the flow rate gradually for both cases. This sudden reduction is corresponding to the onset of elastic turbulence, which has been discussed above.

The HPAM solution with higher salt concentrations induces the elastic turbulence at larger shear rate (flow rate). As shown in the Figure xx, at same flow rate of 20 µl/min, the HPAM solutions with low salinity such as 0.01% and 0.06% are already fully mixed for almost whole channel while for the HPAM solutions with higher salinity, the clear interface is still existing. The numbers of ring with clear interface are also conducted in the Fig. 16. An uptrend is found with the increase of salinity.

Ahead of the occurrence of elastic turbulence, the mixing length increases as the salinity increases, which means less channel rings are dyed at a low flow rate. This is related to effects of the curvature of the geometry discussed above. The addition of the salt leads to the reduction of relaxation time of the polymer solution and its elasticity, making the HPAM solution is hard to induce flow instability at the position close to the inlet of channel. More contributions from the curvilinear channel are required to perturb the stable flow. As a result, the mixing occurs far from the inlet and the mixing length becomes larger.
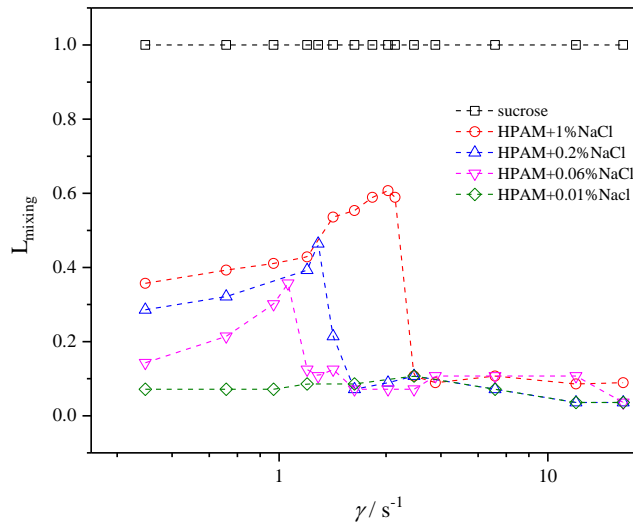
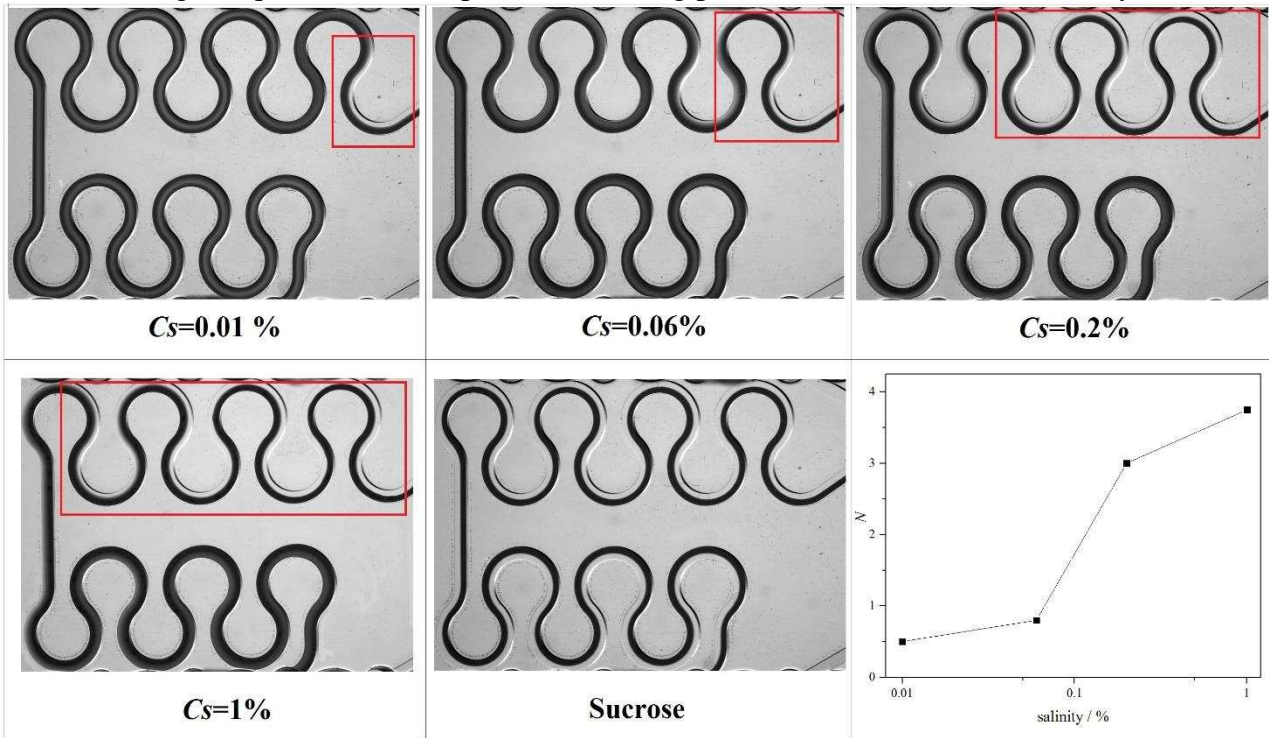Fig. 15 quantitative comparison of mixing performance with different salinty

Fig. 16 Snapshots of mixing performance with different salinities at value of flow rate 20 μl/min

The onset values of shear rate and Weissenberg number at different salt concentrations are performed in the Fig. 17. Similar trends are obtained with the results concluded in swirling flow. The threshold shear rate and Weissenberg number go up to a higher value when the salinity increases. Here, the shear rate of the HPAM solution with 0.01% NaCl is calculated from the minimum applied flow rate (5 μl/min) as no clear interface condition was observed during the experiments. Both the values of shear rate and Weissenberg number are smaller than those in swirling flow due to the discrepancy of the geometry. Indeed, properties of flow dynamics such as PDFs of velocity profiles and power spectra of pressure are both different in these two geometries. Detailed statistical analyses are still under working and will be discussed in the future.
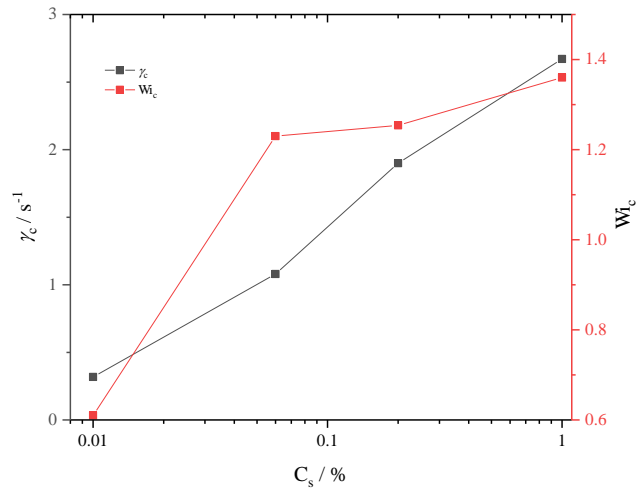
Fig. 17 Salinity effects on the threshold properties of polymer solutions in curvilinear microchannel

6. CONCLUSIONS

The effects of salinity on the onset of elastic turbulence have been investigated experimentally in swirling flow and micro serpentine channels. With increasing the salinity, the polymer relaxation time decreases, resulting in a higher threshold shear rate for the onset of elastic instability. Due to the contribution of shielding effects and poor solvent quality, additional force is required to overcome these suppressions, making the critical Weissenberg number increases as salinity increases. These trends are consistent with the variations of spectra profiles of injected power. A power-law pattern is gradually obverted as the flow transfers from laminar to elastic turbulence, where the exponent increases first and then keeps constant around value of -4.3. In fully developed elastic regime, both this exponent and the normalized peak frequency are independent of salinity. Although high salinity delays the occurrence of elastic turbulence, the growth of flow intensification is more dramatic due to the reduction of the viscosity, accompanied with more intensive skewness of the PDFs of inject power. Similar trends are applied well on the mixing performance and threshold properties in curvilinear microchannel. The discrepancy of the values is ascribed to geometry effects. The diffusion of the fluorescein at low flow rate is possible to indicate the existence of the steady secondary flow instability.

Refrences

(1)   Lumley, J.L.;A.M.J.F. Yaglom, Turbulence;Combustion A century of turbulence. **2001**, 66(3), 241-286.

(2)   Bird, R.B.;R.C. Armstrong;O. Hassager;C.F. Curtiss, Dynamics of polymeric liquids. Vol. 1. 1977: Wiley New York.

(3)   Muller, S.J.;R.G. Larson;E.S.J.R.A. Shaqfeh A purely elastic transition in Taylor-Couette flow. **1989**, 28(6), 499-503.

(4)   Larson, R.G.;E.S. Shaqfeh;S.J.J.J.o.F.M. Muller A purely elastic instability in Taylor–Couette flow. **1990**, 218, 573-600.

(5)   Groisman, A.;V.J.P.o.F. Steinberg Mechanism of elastic instability in Couette flow of polymer solutions: experiment. **1998**, 10(10), 2451-2463.

(6)   Vinogradov, G.;V.J.K.-Z.u.Z.f.P. Manin An experimental study of elastic turbulence. **1965**, 201(2), 93-98.

(7)   Larson, R.G.J.N. Fluid dynamics: turbulence without inertia. **2000**, 405(6782), 27.

(8)   Groisman, A.;V. Steinberg Elastic turbulence in a polymer solution flow. Nature, **2000**, 405(6782), 53-55.

(9)   Groisman, A.;V.J.N. Steinberg Efficient mixing at low Reynolds numbers using polymer additives. **2001**, 410(6831), 905.

(10)   Groisman, A.;V. Steinberg Elastic turbulence in curvilinear flows of polymer solutions. New Journal of Physics, **2004**, 6(1), 29.

(11)   Schiamberg, B.A.;L.T. Shereda;H.U.A. Hu;R.G. Larson Transitional pathway to elastic turbulence in torsional, parallel-plate flow of a polymer solution. Journal of Fluid Mechanics, **2006**, 554(-1), 191.

(12)   Kolmogorov, A.N. The local structure of turbulence in incompressible viscous fluid for very large Reynolds numbers. in Dokl. Akad. Nauk SSSR. 1941.

(13)   Fouxon, A.;V. Lebedev Spectra of turbulence in dilute polymer solutions. Physics of Fluids, **2003**, 15(7), 2060-2072.

(14)   Burghelea, T.;E. Segre;V. Steinberg Role of elastic stress in statistical and scaling properties of elastic turbulence. Phys Rev Lett, **2006**, 96(21), 214502.

(15)   Jun, Y.;V. Steinberg Power and pressure fluctuations in elastic turbulence over a wide range of polymer concentrations. Phys Rev Lett, **2009**, 102(12), 124503.

(16)   Gan, H.Y.;Y.C. Lam;N.-T. Nguyen Polymer-based device for efficient mixing of viscoelastic fluids. Applied Physics Letters, **2006**, 88(22), 224103.

(17)   Gan, H.Y.;Y.C. Lam;N.T. Nguyen;K.C. Tam;C. Yang Efficient mixing of viscoelastic fluids in a microchannel at low Reynolds number. Microfluidics and Nanofluidics, **2006**, 3(1), 101-108.

(18)   Poole, R.J.;B. Budhiraja;A.R. Cain;P.A. Scott Emulsification using elastic turbulence. Journal of Non-Newtonian Fluid Mechanics, **2012**, 177-178, 15-18.

(19)   Clarke, A.;A.M. Howe;J. Mitchell;J. Staniland;L. Hawkes;K. Leeper Mechanism of anomalously increased oil displacement with aqueous viscoelastic polymer solutions. Soft Matter, **2015**, 11(18), 3536-41.

(20)   Howe, A.M.;A. Clarke;D. Giernalczyk Flow of concentrated viscoelastic polymer solutions in porous media: effect of M(W) and concentration on elastic turbulence onset in various geometries. Soft Matter, **2015**, 11(32), 6419-31.

(21)   Mitchell, J.;K. Lyons;A.M. Howe;A. Clarke Viscoelastic polymer flows and elastic turbulence in three-dimensional porous structures. Soft Matter, **2016**, 12(2), 460-8.

(22)   Traore, B.;C. Castelain;T. Burghelea Efficient heat transfer in a regime of elastic turbulence. Journal of Non-Newtonian Fluid Mechanics, **2015**, 223, 62-76.

(23)   Abed, W.M.;R.D. Whalley;D.J.C. Dennis;R.J. Poole Experimental investigation of the impact of elastic turbulence on heat transfer in a serpentine channel. Journal of Non-Newtonian Fluid Mechanics, **2016**, 231, 68-78.

(24)   Li, D.-Y.;X.-B. Li;H.-N. Zhang;F.-C. Li;S.-Z. Qian;S.W. Joo Measuring heat transfer performance of viscoelastic fluid flow in curved microchannel using Ti–Pt film temperature sensor. Experimental Thermal and Fluid Science, **2016**, 77, 226-233.

(25)   Li, D.-Y.;X.-B. Li;H.-N. Zhang;F.-C. Li;S. Qian;S.W. Joo Efficient heat transfer enhancement by elastic turbulence with polymer solution in a curved microchannel. Microfluidics and Nanofluidics, **2017**, 21(1).

(26)   Copeland, D.;C. Ren;M. Su;P.J.I.J.o.H. Ligrani;M. Transfer Elastic turbulence influences and convective heat transfer within a miniature viscous disk pump. **2017**, 108, 1764-1774.

(27)   Ligrani, P.;D. Copeland;C. Ren;M. Su;M.J.J.o.T. Suzuki;H. Transfer Heat Transfer Enhancements from Elastic Turbulence Using Sucrose-Based Polymer Solutions. **2017**, 32(1), 51-60.

(28)   Burghelea, T.;E. Segre;V. Steinberg Elastic turbulence in von Karman swirling flow between two disks. Physics of Fluids, **2007**, 19(5), 053104.

(29)   Burghelea, T.;E. Segre;I. Bar-Joseph;A. Groisman;V. Steinberg Chaotic flow and efficient mixing in a microchannel with a polymer solution. Phys Rev E Stat Nonlin Soft Matter Phys, **2004**, 69(6 Pt 2), 066305.

(30)   Burghelea, T.;E. Segre;V. Steinberg Mixing by polymers: experimental test of decay regime of mixing. Phys Rev Lett, **2004**, 92(16), 164501.

(31)   Belan, S.;A. Chernykh;V.J.J.o.F.M. Lebedev Boundary layer of elastic turbulence. **2018**, 855, 910-921.

(32) Li, X.-B.;M. Oishi;T. Matsuo;M. Oshima;F.-C. Li Measurement of Viscoelastic Fluid Flow in the Curved Microchannel Using Digital Holographic Microscope and Polarized Camera. Journal of Fluids Engineering, **2016**, 138(9), 091401.

(33) Li, X.-B.;M. Oishi;M. Oshima;F.-C. Li;S.-J. Li Measuring elasticity-induced unstable flow structures in a curved microchannel using confocal micro particle image velocimetry. Experimental Thermal and Fluid Science, **2016**, 75, 118-128.

(34) Souliès, A.;J. Aubril;C. Castelain;T. Burghelea Characterisation of elastic turbulence in a serpentine micro-channel. Physics of Fluids, **2017**, 29(8).

(35) Ducloue, L.;L. Casanellas;S.J. Haward;R.J. Poole;M.A. Alves;S. Lerouge;A.Q. Shen;A.J.a.p.a. Lindner Secondary flows of viscoelastic fluids in serpentine microchannels. **2018**.

(36) Scholz, C.;F. Wirner;J.R. Gomez-Solano;C. Bechinger Enhanced dispersion by elastic turbulence in porous media. EPL (Europhysics Letters), **2014**, 107(5), 54003.

(37) Kawale, D.;E. Marques;P.L. Zitha;M.T. Kreutzer;W.R. Rossen;P.E. Boukany Elastic instabilities during the flow of hydrolyzed polyacrylamide solution in porous media: effect of pore-shape and salt. Soft Matter, **2017**, 13(4), 765-775.

(38) Sousa, P.C.;F.T. Pinho;M.A. Alves Purely-elastic flow instabilities and elastic turbulence in microfluidic cross-slot devices. Soft Matter, **2018**, 14(8), 1344-1354.

(39) Ligrani, P.;B. Lund;A. Fatemi Miniature Viscous Disk Pump: Performance Variations From Non-Newtonian Elastic Turbulence. Journal of Fluids Engineering, **2016**, 139(2), 021104.

(40) Lund, B.;P. Ligrani;M. Brown DEVELOPMENT AND CONTROL OF ELASTIC TURBULENCE WITHIN A MICRO-SCALE VISCOUS DISC PUMP. Advances and Applications in Fluid Mechanics, **2016**, 19(3), 517.

(41) Zilz, J.;R.J. Poole;M.A. Alves;D. Bartolo;B. Levaché;A. Lindner Geometric scaling of a purely elastic flow instability in serpentine channels. Journal of Fluid Mechanics, **2012**, 712, 203-218.

(42) Pan, L.;A. Morozov;C. Wagner;P.E. Arratia Nonlinear elastic instability in channel flows at low Reynolds numbers. Phys Rev Lett, **2013**, 110(17), 174502.

(43) Qin, B.;P.E. Arratia Elastic Turbulence in Channel Flows at Low Reynolds number. arXiv preprint arXiv:1609.08532, **2016**.

(44) Qin, B.;P.E. Arratia Characterizing elastic turbulence in channel flows at low Reynolds number. Physical Review Fluids, **2017**, 2(8).

(45) Zhang, H.-N.;F.-C. Li;X.-B. Li;D.-Y. Li;W.-H. Cai;B. Yu Characteristics and generation of elastic turbulence in a three-dimensional parallel plate channel using direct numerical simulation. Chinese Physics B, **2016**, 25(9), 094701.

(46) Latrache, N.;O. Crumeyrolle;I. Mutabazi Transition to turbulence in a flow of a shear-thinning viscoelastic solution in a Taylor-Couette cell. Phys Rev E Stat Nonlin Soft Matter Phys, **2012**, 86(5 Pt 2), 056305.

(47) Malm, A.V.;T.A. Waigh Elastic turbulence in entangled semi-dilute DNA solutions measured with optical coherence tomography velocimetry. Sci Rep, **2017**, 7(1), 1186.

(48) Bodiguel, H.;J. Beaumont;A. Machado;L. Martinie;H. Kellay;A. Colin Flow enhancement due to elastic turbulence in channel flows of shear thinning fluids. Phys Rev Lett, **2015**, 114(2), 028302.

(49) Fardin, M.A.;D. Lopez;J. Croso;G. Gregoire;O. Cardoso;G.H. McKinley;S. Lerouge Elastic turbulence in shear banding wormlike micelles. Phys Rev Lett, **2010**, 104(17), 178303.

(50) Li, F.-C.;H. Kinoshita;X.-B. Li;M. Oishi;T. Fujii;M. Oshima Creation of very-low-Reynolds-number chaotic fluid motions in microchannels using viscoelastic surfactant solution. Experimental Thermal and Fluid Science, **2010**, 34(1), 20-27.

(51) Majumdar, S.;A.K. Sood Universality and scaling behavior of injected power in elastic turbulence in wormlike micellar gel. Phys Rev E Stat Nonlin Soft Matter Phys, **2011**, 84(1 Pt 2), 015302.

(52) Beaumont, J.;N. Louvet;T. Divoux;M.-A. Fardin;H. Bodiguel;S. Lerouge;S. Manneville;A. Colin Turbulent flows in highly elastic wormlike micelles. Soft Matter, **2013**, 9(3), 735-749.

(53) Casanellas, L.;M.A. Alves;R.J. Poole;S. Lerouge;A. Lindner The stabilizing effect of shear thinning on the onset of purely elastic instabilities in serpentine microflows. Soft Matter, **2016**, 12(29), 6167-75.

(54) Schweins, R.;J. Hollmann;K.J.P. Huber Dilute solution behaviour of sodium polyacrylate chains in aqueous NaCl solutions. **2003**, 44(23), 7131-7141.

(55) Gerashchenko, S.;C. Chevallard;V. Steinberg Single-polymer dynamics: Coil-stretch transition in a random flow. Europhysics Letters (EPL), **2005**, 71(2), 221-227.

(56) Yao, G.;J. Zhao;S.B. Ramisetti;D. Wen Atomistic Molecular Dynamic Simulation of Dilute Poly(acrylic acid) Solution: Effects of Simulation Size Sensitivity and Ionic Strength. Industrial & Engineering Chemistry Research, **2018**, 57(50), 17129-17141.

(57) Wu, C.;K.K. Chan;K.-Q.J.M. Xia Experimental study of the spectral distribution of the light scattered from flexible macromolecules in very dilute solution. **1995**, 28(4), 1032-1037.

(58) Pohlmeier, A.;S.J.J.o.c. Haber-Pohlmeier;i. science Ionization of short polymethacrylic acid: titration, DLS, and model calculations. **2004**, 273(2), 369-380.

(59) Satoh, K.;S. Kuroki;M.J.C. Satoh;P. Science Charge density-dependent coil–globule transition of alkali metal polycarboxylates in aqueous organic solvent mixtures. **2013**, 291(6), 1453-1462.

(60)   Takani, S.;M.J.J.o.M.S. Satoh, Part B Temperature-induced coil-globule transition of alkali metal polyacrylates in aqueous organic solvent mixtures. **2016**, 55(9), 955-967.

(61)   Jun, Y.;V. Steinberg Polymer concentration and properties of elastic turbulence in a von Karman swirling flow. Physical Review Fluids, **2017**, 2(10).